Co-published by
Institute of Fluid-Flow Machinery
Polish Academy of Sciences
Committee on Thermodynamics and Combustion
Polish Academy of Sciences

http://www.imp.gda.pl/archives-of-thermodynamics/

Pool boiling for water on surfaces with inclined microchannel

Robert Mikołaj Kaniowski[a*]

[a]Kielce University of Technology, Faculty of Mechatronics and Mechanical Engineering,
al. Tysiąclecia Państwa Polskiego 7, 25-314 Kielce, Poland
*Corresponding author email: kaniowski@tu.kielce.pl

Received: 19.12.2023; revised: 12.03.2024; accepted:09.05.2024

Abstract

The heat transfer measurements were conducted during pool boiling of water on surfaces with microchannels. Parallel grooves were made on a copper surface with widths ranging from 0.2 mm to 0.5 mm at intervals of 0.1 mm. The inclination angle of the grooves to the horizontal was set at 30° and 60°, and the depth of the microchannel grooves was 0.3 mm. The achieved heat flux ranged from 25 kW/m² to 1730 kW/m², and the heat transfer coefficients ranged from 12 kW/(m²K) to 475 kW/(m²K). The influence of geometric parameters such as width, inclination angle of the microchannel, surface extension, and Bond number on heat exchange efficiency was examined. A nearly sixfold increase in α (heat transfer coefficient) and a twofold increase in critical heat flux were observed compared to a smooth surface.

Keywords: Pool boiling; Inclined microchannel; Heat transfer coefficient; Critical heat flux

Vol. 45(2024), No. 2, 41–49; doi: 10.24425/ather.2024.150850

Cite this manuscript as: Kaniowski, R.M. (2024). Pool boiling for water on surfaces with inclined microchannel. *Archives of Thermodynamics*, 45(2), 41–49.

1. Introduction

The machinery employed in the power sector is engineered to function within a designated temperature range. To maintain optimal operating temperatures for its components, it is crucial to employ appropriate heat exchangers and heat spreaders. These devices utilize specialized surfaces to enhance both the heat transfer coefficient and the dissipation of heat flux. Leveraging the heat of vaporization during boiling facilitates the efficient removal of substantial heat loads while minimizing the required heat exchange surface. To meet criteria for lightweight design and device compatibility, dual-phase heat exchangers and dissipators are employed for effective heat dispersion [1]. These systems find applications in both industrial equipment and scientific test benches. There is also a growing interest in the development of miniature cooling technologies using passive methods such as boiling in closed devices, such as immersion cooling thermosyphons, pulsating heat pipes, and two-phase heat spreaders, etc. [2]. One of the most efficient and versatile methods of increasing the heat transfer coefficient and critical heat flux during boiling is the use of the appropriate fluid and surface type. Surface modifications can consist of texturing, perforation application, subsurface tunnel formation, porous layer coating, creation of metal foams, mesh, perforation, notching of small ribs or microchannels, etc. The two methods of creating surfaces with microchannels analysed in the publication [3], parallel and cross, demonstrated the influence of configuration on heat

Nomenclature

A – area, m^2
a – width of specimen, m
Bo – Bond number
b – angle, °
c_p – specific heat, J/(kg K)
d – diameter, m
g – gravitational acceleration, m/s^2
h – microchannel depth, m
i – enthalpy, kJ/kg
L – length, m
q – heat flux, W/m^2
p – pitch, m
Ra – roughness, μm
T – temperature, K
U – perimeter, m
u – velocity, m/s
w – width, m

Greek symbols

α – heat transfer coefficient, W/(m^2 K)
Δ – error, uncertainty
ΔT – superheat referred to the microfin base, K
δ – distance, m
φ – surface extension
λ – thermal conductivity, W/(m K)
ρ – density, kg/m^3
σ – surface tension, N/m
υ – kinematic viscosity, m^2/s

Subscripts and Superscripts

bs – base
Cu – copper
cap – capillary
cyl – cylinder
ext – extended
h – hydraulic
l – liquid
max – maximum
sat – saturated
$T1, ..., T8$ – thermocouple number
v – vapour

exchange efficiency. This study also examined the effect of material division and material proportions for the parallel configuration, and the effect of division for the cross configuration. The authors have demonstrated that the heat transfer performance is higher for surfaces with a fin arrangement in a cross-flow configuration compared to a parallel configuration.

One effective way to intensify heat transfer in boiling is to increase the number of nucleation sites and ensure their continuous operation [4]. Metals are suitable for this purpose, especially those with a high heat transfer coefficient and at a relatively low price [5]. Another way to improve the heat transfer coefficient is to use other coolants, i.e. water with added nanoparticles, water – Al_2O_3 or water – Cu, and to increase operating pressure [6]. Also being developed are enhanced industrial surfaces GEWA-B5, GEWA-KS, and EHPII coated with nanostructures, which have been described and examined in the work of Dickson et al. [7]. The studies [8,9] also examined how the spatial orientation of minichannels affects the boiling process when FC-72 coolant flows. The tested surfaces were made of Haynes-230 alloy. The following methods were used to develop the heat exchange surface: electro-machining texturing (erosion), laser surface texturing (laser), porous surface produced by soldering iron powder (porous), produced with the use of emery papers of varying roughness.

The subject of the research in the [10] paper by Khalaf-Allah et al. was water at atmospheric pressure on surfaces fabricated by multi-passive techniques. Experiments were conducted in a saturated pool boiling state for heat fluxes ranging from 50 to 580 kW/m^2. The results showed that a maximum improvement of 51–92% could be achieved with the composite surface compared to the smooth surface. Orman et al. [11] examined pool boiling on surfaces featuring microchannels created with lasers. They conducted experiments using water and ethanol under atmospheric pressure. The most effective results were observed on surfaces with microchannels characterized by greater depth and narrower dimensions. Zhang et al. in [12] conducted a heat transfer study on finned surfaces coated with a porous structure consisting of ball-shaped powder with a diameter of 380–550 μm. The boiling medium was water. The heat transfer coefficient decreased with the increase in microporous plate diameter, while it increased with the increase in thickness of the porous copper plate. The paper by Liang and Mudawar [13] presents the results of an experimental study of passive cooling for different types of heating surface modification techniques. One of the techniques used is the production of micro fins and microchannels. These areas have great potential due to the significant increase in CHF (critical heat flux) and the increase in the number of nucleation sites.

Surfaces subjected to micro-processing significantly improve the heat transfer efficiency during pool boiling. Liu et. al. [14] investigated the performance on five micro/nanostructured surfaces. For all structural surfaces, the results show an increase in the heat transfer coefficient. The critical heat flux and the heat transfer coefficient were increased to 60% and 331%, respectively. The authors in [15] experimentally investigated bistructural surfaces based on micro-pin-finned ribbing methods. Compared to smooth surfaces, dual-textured surfaces increased critical heat flow by more than 120%.

Gheitaghy et al. [16] investigated the boiling process of distilled water under atmospheric pressure. The study explores the impact of surface structuring using vertical, inclined, and orthogonal minichannels on pool boiling. The dimensions of inclined minichannels, varying from 0.5 mm to 1.4 mm, were systematically altered. In addition to augmenting the surface area, improvements in boiling performance were achieved by increasing minichannel depth and reducing pitch. Practical surface structuring of inclined minichannels was accomplished through the EDM (electrical discharge machining) method. The study

revealed a 2.7-fold increase in the heat transfer coefficient compared to a smooth surface and a 65% enhancement in critical heat flux.

The paper provides a concise summary of experimental results concerning heat exchange under pool boiling of water. The study aimed to identify the most favorable microchannel geometry to achieve the highest heat transfer coefficients and critical heat flux values.

2. Materials and methods

The experimental setup described in reference [17], as illustrated in Fig. 1, enabled the determination of boiling curves under increasing heat flux conditions. The research involved experimental investigations into heat transfer on inclined microchannels, covering the range from the onset of nucleate boiling (ONB) to the initial boiling crisis in pool boiling. All tests were conducted under atmospheric pressure.

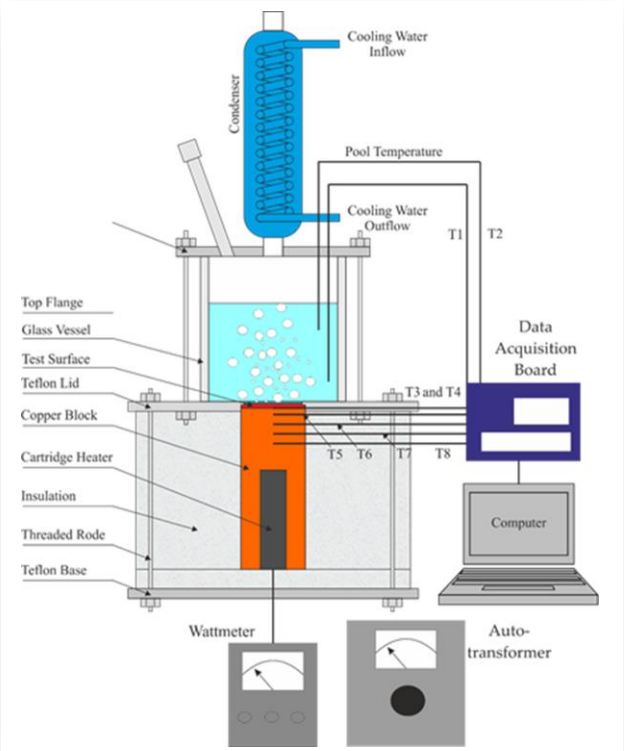

Fig. 1. Test stand diagram.

The measurement process commenced by initiating the water cooler to generate condensate from vaporized boiling water. Subsequently, the heating circuit was activated, and the fluid was heated until it reached the saturation state. This condition was maintained for the following 10 minutes (water degassing). Sequentially, the suitable electric voltages were applied to the autotransformer (simulating the desired heat flow value), and a waiting period of approximately 15 minutes ensued until the system achieved thermal equilibrium (temperature readings remained constant for the subsequent 5 minutes).

Data registration was carried out on the Fluke Hydra Series II 2635A data acquisition station (temperatures on the copper heating rod T3 to T8, liquid saturation temperatures T1 and T2). K-type thermocouples with a protective sheath and a diameter of 0.5 mm were employed for temperature measurements. Before conducting the measurements, calibration of the thermocouples was performed using an Altek 422 calibrator. The sensors underwent testing within the temperature range of 90°C to 300°C at intervals of 5°C. The absolute error of the thermocouple did not surpass 0.1 K.

In order to maintain consistency in experimental investigations and reduce errors associated with the determination of heat flow and heat transfer coefficient, the equation for one-dimensional heat conduction was utilized. The heating cylinder was insulated with a substantial layer, effectively preventing lateral heat transfer. Consequently, the calculations for heat flux adhere to the principles of Fourier's law:

$$q = \lambda_{\mathrm{Cu}} \frac{T_{T8}+T_{T5}}{\delta_{T8-T5}} \frac{\pi d_{cyl}^2}{4a^2}. \tag{1}$$

The distance between the thermocouples, as shown in Fig. 2, is $\delta_{T8\text{-}T5}$ = 35mm, the diameter of the copper cylinder d_{cyl} = 45 mm and the active side of the sample a = 37 mm. Thermal conductivity of copper adopted is 380 W/(m K).

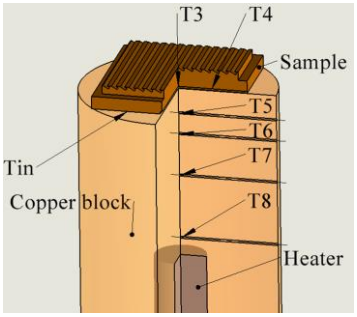

Fig. 2. Distribution of temperature sensors along the heating cylinder.

The heat transfer coefficient α between the surface with incised inclined microchannels and the fluid was determined from the relationship

$$\alpha = \frac{q}{\Delta T} \tag{2}$$

with the temperature difference determined, according to Figs. 1 and 2, as

$$\Delta T = \frac{T_{T3}+T_{T4}}{2} - q \frac{\delta_{bs}}{\lambda_{Cu}} \frac{T_{T1}+T_{T2}}{2}. \tag{3}$$

The distance between the base of the sample and the bottom of the microchannel δ_{bs} for each sample was different and was determined as shown in Fig. 3. It also shows the characteristic dimensions of the developed area.

Water provides the highest heat transfer coefficients and the highest critical heat fluxes. However, its saturation temperature, at atmospheric pressure, is high and cannot be used to directly cool certain components, e.g. microprocessors. This fluid can be used in demineralized form because otherwise there could be

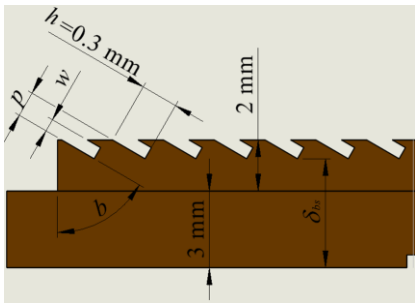

Fig. 3. Characteristic dimensions of the unfolded surface.

a likelihood of channel blockage by sediments. Physical properties of water in a saturated state, necessary for calculations, are presented in Table 1.

Table 1. Water properties.

Parameters under normal pressure	
T_{sat}, °C	100
ρ_l, kg/m³	959
ρ_v, kg/m³	0.597
i_{lv}, kJ/kg	2257
λ_l, W/(m·K)	0.68
σ_l, N/m	0.0589
μ_l, Pa·s	0.00028
c_{pl}, J/(kg K)	4220

The surfaces subjected to testing were constructed from copper, possessing a thermal conductivity of 380 W/(m K). The test specimens (Fig. 4) were surfaces with incised inclined microchannels and a reference smooth surface with a roughness of Ra = 0.12 µm. Incisions on the specimens were made with disc cutters with a width of w = 0.5 mm to 0.2 mm in 0.1 mm increments, to a depth of h = 0.3 mm (as shown in Fig. 3) and an angle to the vertical of b = 30° and 60°. Unfortunately, the technological process of producing the [18] surface results in slight deficiencies on the surface related to surface roughness and the fabrication of microchannels. All specimens were made with a similar face roughness of approximately 0.2 µm. Table 2 presents codes and specifications for the specimens.

Table 2. Specimen codes and specifications.

Specimen code	w, mm	h, mm	p, mm	b,°
M2.3-30	0.20	0.30	0.40	30
M3.3-30	0.30	0.30	0.60	30
M4.3-30	0.40	0.30	0.80	30
M5.3-30	0.50	0.30	1.00	30
M2.3-60	0.20	0.30	0.40	60
M3.3-60	0.30	0.30	0.60	60
M4.3-60	0.40	0.30	0.80	60
M5.3-60	0.50	0.30	1.00	60

Using a complete differential error, the uncertainty of the heat flux measurement was determined:

$$\Delta q = (A^2 + B^2 + C^2 + D^2 + E^2)^{0.5}, \tag{4}$$

whereas the individual components are equal to:

$$A = \frac{\partial q}{\partial \lambda}\Delta\lambda, \tag{4a}$$

$$B = \frac{\partial q}{\partial \Delta T_{T5-T8}}\Delta\left(\Delta T_{T5-T8}\right), \tag{4b}$$

$$C = \frac{\partial q}{\partial \Delta \delta_{T5-T8}}\Delta\delta_{T5-T8}, \tag{4c}$$

$$D = \frac{\partial q}{\partial d_{cyl}}\Delta d_{cyl}, \tag{4d}$$

$$E = \frac{\partial q}{\partial a}\Delta a. \tag{4e}$$

Here the thermal conductivity coefficient $\Delta\lambda$ = 1 W/(m K), the temperature difference in the heating cylinder and the wall superheat error are assumed to be 0.2 K, and length and diameter measurements $\Delta\delta_{T5\text{-}T8} = \Delta d_{cyl} = \Delta a = 2.5\times10^{-4}$ m (calipers for precision).

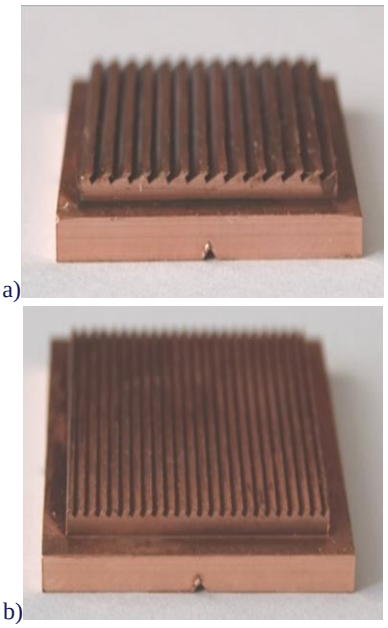

Fig. 4. Example surface images: a) M5.3-60, b) M5.3-30.

The relative error in the measurement of heat flux density between 25 kW/m² and 1730 kW/m² took values between 11.5% and 2.3%. In the analytical considerations, the thickness of the tin and the error associated with its conductivity have been ignored, due to the fact that their values are very small and do not affect the overall result. The largest measurement errors occur at low heat fluxes due to the gradient method of determining the heat flux density used, i.e. a significant absolute error in temperature measurement is generated at low superheats.

The absolute current of the heat transfer coefficient $\Delta\alpha$ was determined using the relationship

$$\Delta\alpha = \left[\left(\frac{\partial\alpha}{\partial q}\Delta q\right)^2 + \left(\frac{\partial\alpha}{\partial\Delta T}\Delta(\Delta T)\right)^2\right]^{0.5} \quad (5)$$

with the absolute error of overheating determined by the formula

$$\Delta(\Delta T) = \left[\left(\frac{\partial\Delta(\Delta T)}{\partial q}\Delta q\right)^2 + \left(\frac{\partial\Delta(\Delta T)}{\partial\Delta T_{sat}}\Delta(\Delta T_{sat})\right)^2 + \right.$$
$$\left. + \left(\frac{\partial\Delta(\Delta T)}{\partial\lambda}\Delta\lambda\right)^2 + \left(\frac{\partial\Delta(\Delta T)}{\partial\delta_{bs}}\Delta\delta_{bs}\right)^2\right]^{0.5}. \quad (6)$$

The outcomes and the procedure for identifying errors align with those outlined in Jaikumar and Kandlikar [19] as well as Kaniowski and Pastuszko [20]. The assessment involved estimating the relative error in determining the heat transfer coefficient, as influenced by the heat flux and superheat (refer to Eq. (5)). The relative error in determining the heat transfer coefficient, spanning from 12 kW/(m^2 K) to 475 kW/(m^2 K), varied between 5.4% and 36.2%.

3. Results and discussion

Experimental heat transfer studies were carried out for deionized water during bubble boiling on a smooth, flat surface and on surfaces with inclined microchannels at atmospheric pressure. Experiments were performed with increasing heat flux density. Heat transfer as a complex phenomenon during boiling in a large volume involves the following basic mechanisms: evaporation of the liquid microlayer, forced convection and heat conduction [21]. Figure 5 shows the boiling curves for all the surfaces analysed. An almost twofold increase in critical heat flux is evident for almost every surface. Only for a surface with a microchannel width of 0.2 mm is the critical heat flux higher by approx. 67% and for sample MC5.3-30 by approx. 44%.

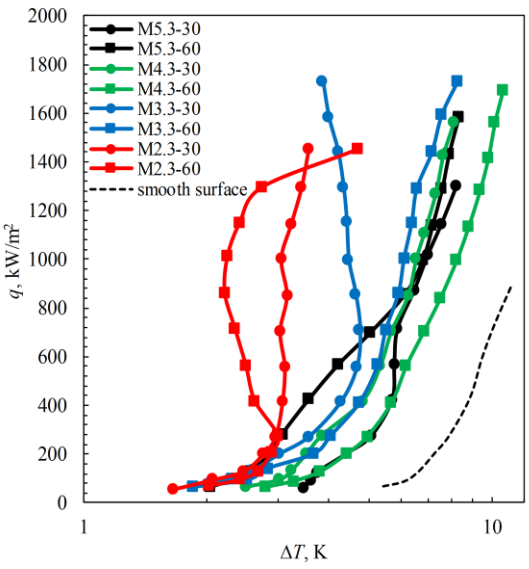

Fig. 5. Boiling curves for the analyzed surfaces.

The impact of the micro-groove's inclination angle relative to the vertical on the heat transfer process was examined. The most favorable outcomes were observed for surfaces with microchannels inclined at 60°, designated as M2.3-60. The heat transfer coefficient reached 475 kW/m^{2}K with a heat flux of 1146 kW/m^2 and a superheat of $\Delta T \approx 2.4$ K, as illustrated in Fig. 5. A notable 5.9-fold increase in the heat transfer coefficient was achieved compared to the smooth sample, as shown in Fig. 6. As the width of the microchannel increases, there is a discernible downward trend in the efficiency of heat transfer. The enhancement of the heat transfer mechanism for surfaces with microchannels occurs when the number of nucleation sites in the channels increases with a small temperature difference (overheating).

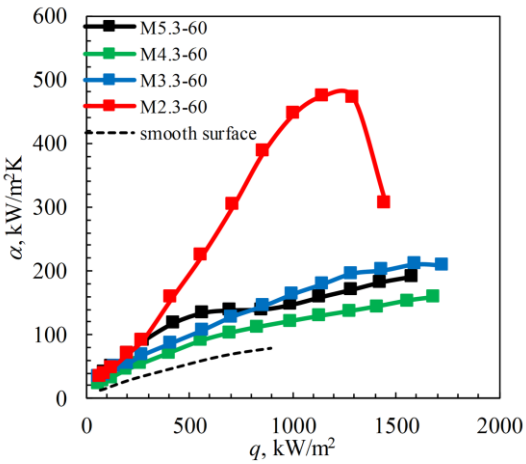

Fig. 6. Heat transfer coefficient vs. heat flux, b = 60°.

Among the various surfaces, those with microchannels featuring a width of 0.2 mm and an inclination angle of 60° demonstrated the highest efficiency. This could be attributed to the enlarged heat transfer surface area and the filling of microchannels by the boiling medium. It's worth noting that, in contrast, Gheitaghy et al. [16] achieved notably superior results for surfaces with channels inclined at 45° in their study. The heat transfer coefficient initially rises and then falls with the temperature difference, reaching a maximum corresponding to a change in slope in the boiling curve. This peak is a common occurrence in pool boiling with finned surfaces. This phenomenon is associated with the transition between two regimes of pool boiling. At low wall superheat, bubble columns form at specific nucleation sites, and their dynamics are independent of neighboring columns. Following the increase in wall temperature, the entire heated surface becomes involved in nucleation, leading to an increase in interaction between the bubble columns. Consequently, the likelihood of fresh fluid flowing to the heated finned surface decreases, resulting in a decrease in heat transfer [21,22].

The surfaces that have been examined combine various methods of enhancing heat transfer. One of the methods involves macroconvection during the flow of liquid and vapor through the microchannel. This leads to enhancements in critical

heat flux and heat transfer coefficients. Additionally, the surfaces feature finned walls that increase surface area, thereby intensifying liquid convection. This, in turn, enhances liquid evaporation and reduces wall overheating, ultimately facilitating improved heat transfer.

Microchannels with a width of 0.3 mm exhibit the highest critical heat flux values, approximately 93% greater than those of the smooth surface. However, their heat transfer coefficients vary significantly depending on the angle of the microchannels relative to the vertical.

From the 0.5 mm and 0.4 mm wide microsurfaces analysed experimentally, it is clear that the inclination of the microchannels does not matter, as the results of the heat transfer coefficients are almost identical. Only in the initial phase of the heat flux increase for a width of 0.5 mm, up to 700 kW/m^2, there is a 60% decrease in heat transfer coefficient to the detriment of a surface with a 30° inclination of the microchannels, Fig. 7.

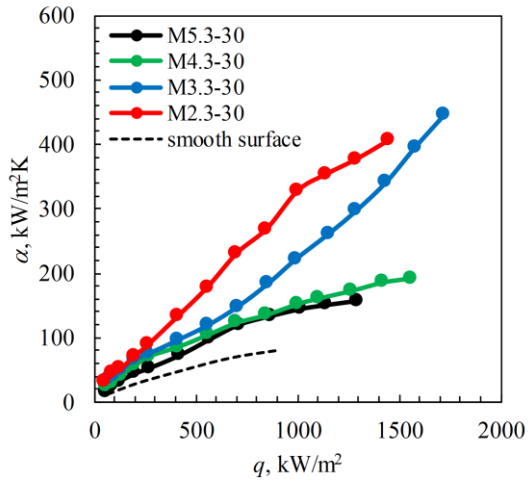

Fig. 7. Heat transfer coefficient vs. heat flux, b = 30°.

More boiling nucleation sites and a larger heat transfer surface area result in an increase in heat transfer coefficient and critical heat flux [23]. One of the parameters describing the surface is the surface extension:

$$\varphi = \frac{A_{\text{ext}}}{A_{\text{smooth}}} = \frac{2h+w\left[1-\tan(b)+\frac{1}{\cos(b)}\right]}{p}. \tag{7}$$

Another parameter is the Bond number, which involves a comparison between two forces: gravity and forces associated with surface tension. A high Bond number indicates the dominance of gravitational forces, while a low Bond number signifies the prevalence of surface tension forces. Below is the relationship for the Bond number [24]:

$$\text{Bo} = \frac{g\rho d_h^2}{\sigma} = \left(\frac{d_h}{L_{cap}}\right)^2, \tag{8}$$

where the hydraulic diameter is specified as

$$d_h = \frac{4A}{U} = \frac{2w[2h-w\tan(b)]}{2h+w\left[1-\tan(b)+\frac{1}{\cos(b)}\right]}, \tag{9}$$

while the capillary length is

$$L_{cap} = \sqrt{\frac{\sigma}{g(\rho_l-\rho_v)}}. \tag{10}$$

Table 3 shows the results of the surface extension, hydraulic diameter, and Bond number calculations. The geometric parameters in Table 1 were used to determine the hydraulic diameter. These values vary from 0.27 mm to 1.26 mm.

Table 3. Calculated values of surface and fluid properties.

Specimen code	φ	d_h, mm	Bo
M2.3-30	2.29	1.26	0.504
M3.3-30	1.79	1.02	0.408
M4.3-30	1.54	0.82	0.330
M5.3-30	1.39	0.66	0.262
M2.3-60	2.13	1.24	0.497
M3.3-60	1.63	0.91	0.362
M4.3-60	1.38	0.58	0.233
M5.3-60	1.23	0.27	0.108

Utilizing the outcomes of surface extension and Bond number computations, the features of critical heat flux and maximum heat transfer coefficients were established, as depicted in Figs. 8 and 9. In both microchannel angles, an initial rise in critical flux with an increase in surface area and Bond number, respectively, is evident, followed by a subsequent decline. This is not in line with the research carried out in [25]. In contrast, the effect of φ and Bo$^{0.5}$ on the heat transfer coefficient is consistent, Fig. 9. The capillary pressure in the space between the fins increases with increasing surface area, resulting in significant resistance to fluid flow in the microchannel and a reduction in critical heat flux. This affects the drying out of the spaces in the microchannel. The width and spacing of the microgrooves can also have a significant effect on heat transfer efficiency, as increasing the channel width affects the coalescence of vapour bubbles. The narrower the channel, the greater the potential for blister bonding at high heat flux [26].

The Reynolds number was determined because the boiling of the fluid causes it to be in motion in a confined space, which is the microchannel. This figure provides an estimate of the ratio of inertial to viscous forces occurring during fluid movement:

$$\text{Re} = \frac{uL_{cap}}{\upsilon_l}. \tag{11}$$

Assuming that all of the heat is dissipated by the latent heat of vaporization, the vapor velocity is

$$u = \frac{q}{i_{lv}\rho_v}. \tag{12}$$

Combining Eqs. (11)–(12) yields an expression for Re:

$$\text{Re} = \frac{qL_{cap}}{i_{lv}\rho_v\upsilon_l}. \tag{13}$$

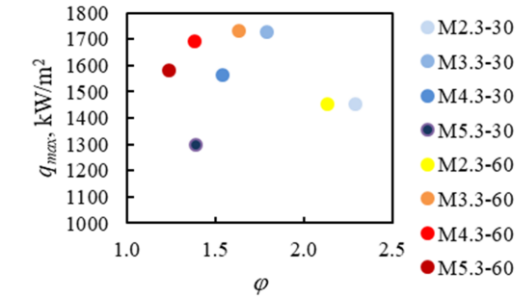

a)

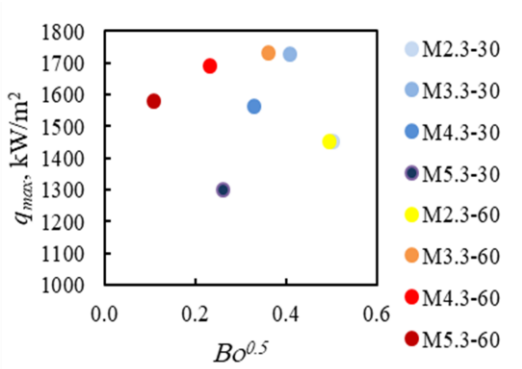

b)

Fig. 8. Variation of critical heat flux with
a) surface extension coefficient, b) $Bo^{0.5}$ for microchannel.

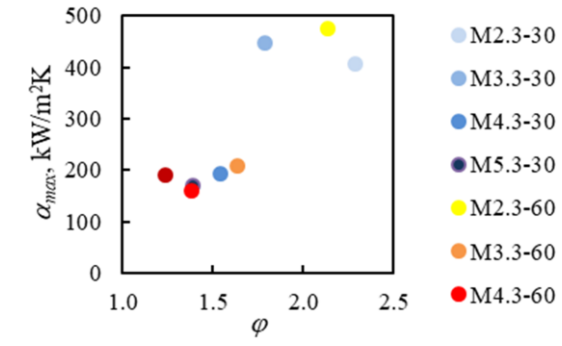

a)

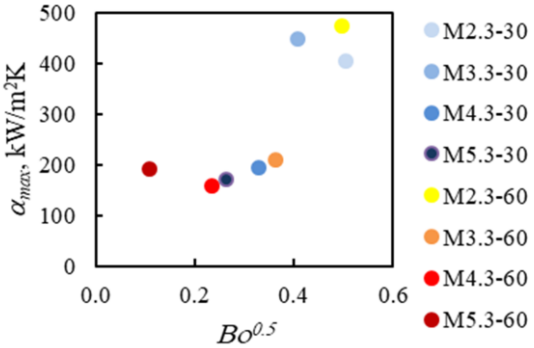

b)

Fig. 9. Variation of heat transfer coefficient with
a) surface extension coefficient, b) $Bo^{0.5}$ for microchannel.

The effect of the Reynolds number on the maximum heat transfer coefficient is shown in Fig. 10. The fluid flows through the microchannels are not large, 8200 < Re < 11000, so the friction factor is large. This has implications for the effective flooding of the microchannel.

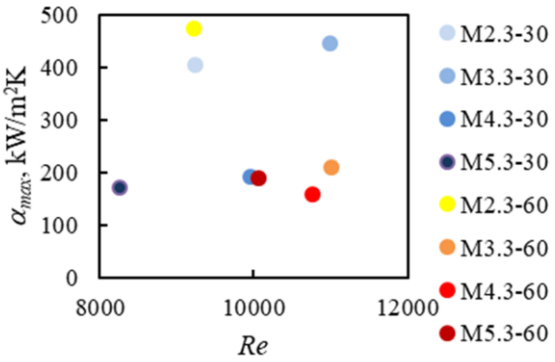

Fig. 10. Variation of heat transfer coefficient
with Reynolds number.

In order to obtain a benchmark for the heat transfer efficiency of the surfaces produced, a comparison is made with experimental studies reported in the literature for saturated pool boiling of water at atmospheric pressure. Figure 11 shows the boiling curves of other authors Gheiaghty et al. [16], Gouda et al. [26], Jaikumar and Kandlikar [19], Walunj and Sathyabhama [27], Zhang et al. [12], and the curve with the best heat transfer efficiency – surface M#2.3-60. The maximum heat flux results, especially for Jaikumar and Kandlikar [19], have almost twice the critical heat flux value, while the superheat values are significantly higher, which is unfavourable. This may be due to the specific and significant development of the surface (skewed microchannels, expansion of the surface).

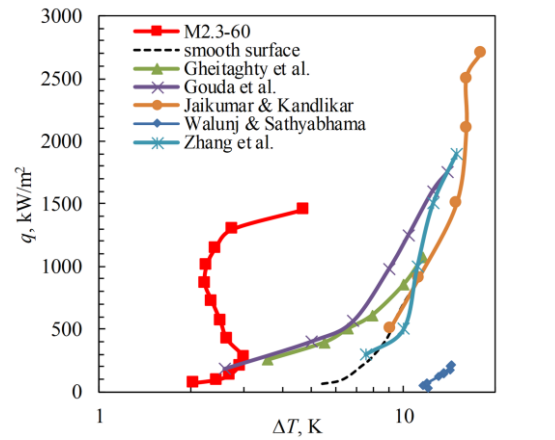

Fig. 11. Boiling curve comparison for other structures in literature.

6. Conclusions

Surfaces with microchannels provide higher heat transfer coefficients compared to smooth surfaces and are easy to produce consistently through subtractive manufacturing processes. The samples tested with microchannels exhibited a notable increase in heat transfer with the heat transfer coefficient dependent on both the angle of inclination to the horizontal and the width of the microchannel. The maximum observed heat flux reached 1730 kW/m^2, while the heat transfer coefficient was 475 kW/(m^2 K). In comparison to a smooth surface, the maximum heat flux nearly doubled, and the heat transfer coefficient was 5.9 times higher.

The largest heat transfer coefficients were achieved with the largest extensions of microchannel surfaces, specifically those with the narrowest microchannel widths. This characteristic contributed to the creation of a substantial number of active nucleation sites at the bottom and lateral surfaces of the microchannels. Comparing boiling curves highlighted the influence of microchannel width and angle on the boiling process.

Understanding the heat transfer coefficient and critical heat flow parameters is crucial in the development of heat spreaders, underscoring the importance of creating new surfaces and heat-receiving fluids.

Acknowledgements

The research reported in this article was partially supported by a grant from Poland's Minister of Education and Science through the Poland's Metrology Program [Polska Metrologia]. Grant Number: PM/SP/0031/2021/1.

References

[1] Liang, G., & Mudawar, I. (2018). Pool boiling critical heat flux (CHF) – Part 1: Review of mechanisms, models, and correlations. *International Journal of Heat and Mass Transfer*, 117, 1352–1367. doi: 10.1016/ j.ijheatmasstransfer.2017.09.134

[2] Moon, J.H., Fadda, D., Shin, D.H., Kim, J.S., Lee, J., & You, S.M. (2021). Boiling-driven, wickless, and orientation-independent thermal ground plane. *International Journal of Heat and Mass Transfer*, 167, 120817. doi: 10.1016/j.ijheatmasstransfer.2020.120817

[3] Chen, Z., Xie, T., & Utaka, Y. (2023). Enhanced critical heat flux in pool boiling applying the method of different-mode-interacting boiling for water. *International Journal of Heat and Mass Transfer*, 201, 123578. doi: 10.1016/j.ijheatmasstransfer.2022.123578

[4] Chuang, T.J., Chang, Y.H., & Ferng, Y.,M. (2019). Investigating effects of heating orientations on nucleate boiling heat transfer, bubble dynamics, and wall heat flux partition boiling model for pool boiling. *Applied Thermal Engineering*, 163, 114358. doi: 10.1016/j.applthermaleng.2019.114358

[5] Qu, Z.G., Xu, Z.G., Zhao, C., Y., & Tao, W.Q. (2012). Experimental Study of pool boiling heat transfer on horizontal metallic foam surface with crossing and single-directional V-shaped groove in saturated water. *International Journal of Multiphase Flow*, 41, 44–55. doi: 10.1016/j.ijmultiphaseflow.2011.12.007

[6] Cieśliński, J., & Kaczmarczyk, T. (2014). Pool boiling of nanofluids on rough and porous coated tubes: experimental and correlation. *Archives of Thermodynamics*, 35, 3–20. doi: 10.2478/aoter-2014-0010

[7] Dickson, D., Bock, B.D., & Thome, J.R. (2024). Heat transfer of uncoated and nanostructure coated commercially micro-enhanced refrigeration tubes under pool boiling conditions. *Applied Thermal Engineering*, 236, 121757. doi: 10.1016/j.applthermaleng.2023.121757

[8] Piasecka, M., Strąk, K., & Maciejewska, B. (2021). Heat transfer characteristics during flow along horizontal and vertical minichannels. *International Journal of Multiphase Flow*, 137, 103559. doi: 10.1016/j.ijmultiphaseflow.2021.103559

[9] Piasecka, M., & Strąk, K. (2022). Boiling heat transfer during flow in vertical mini-channels with a modified heated surface. *Energies*, 15, 7050. doi: 10.3390/en15197050

[10] Khalaf-Allah, R.A., Mohamed, S.M., Saeed, E., & Tolan, M. (2023). Augmentation of water pool boiling heat transfer using heating surfaces fabricated by multi passive techniques. *Applied Thermal Engineering*, 219, 119693. doi: 10.1016/j.applthermaleng.2022.119693

[11] Orman, Ł.J., Radek, N., Pietraszek, J., & Szczepaniak, M. (2020). Analysis of enhanced pool boiling heat transfer on laser-textured surfaces. *Energies*, 13, 1–19. doi: 10.3390/en13112700

[12] Zhang, K., Bai, L., Lin, G., Jin, H., & Wen, D. (2019). Experimental study on pool boiling in a porous artery structure. *Applied Thermal Engineering*, 149, 377–384. doi: 10.1016/j.applthermaleng.2018.12.089

[13] Liang, G., & Mudawar, I. (2019). Review of pool boiling enhance-ment by surface modification. *International Journal of Heat and Mass Transfer*, 128, 892–933. doi: 10.1016/j.ijheatmasstransfer.2018.09.026

[14] Liu, B., Cao, Z., Zhang, Y., Wu, Z., Pham, A., Wang, W., Yan, Z., Wei, J., & Sundén, B. (2018). Pool boiling heat transfer of N-pentane on micro/nanostructured surfaces. *International Journal of Thermal Sciences*, 130, 386–394. doi: 10.1016/j.ijthermalsci.2018.05.012

[15] Kong, X., Zhang, Y., & Wei, J. (2018) Experimental study of pool boiling heat transfer on novel bistructured surfaces based on micro-pin-finned structure. *Experimental Thermal and Fluid Science*, 91, 9–19. doi: 10.1016/j.expthermflusci.2017.09.021

[16] Gheitaghy, A.M., Samimi, A., & Saffari, H. (2017). Surface structuring with inclined minichannels for pool boiling improvement. *Applied Thermal Engineering*, 126, 892–902. doi: 10.1016/j.applthermaleng. 2017.07.200

[17] Kaniowski, R., & Pastuszko, R. (2023). Pool boiling experiment with Novec-649 in microchannels for heat flux prediction. *Experimental Thermal and Fluid Science*, 141, 110802. doi: 10.1016/j.expthermflusci. 2022.110802

[18] Skrzyniarz, M., Nowakowski, L., Miko, E., & Borkowski, K. (2021). Influence of relative displacement on surface roughness in longitudinal turning of X37CrMoV5-1 steel. *Materials*, 14, 1317. doi: 10.3390/ma14051317

[19] Jaikumar, A., & Kandlikar, S.G. (2016). Ultra-high pool boiling performance and effect of channel width with selectively coated open microchannels. *International Journal of Heat and Mass Transfer*, 95, 795–805. doi: 10.1016/j.ijheatmasstransfer.2015.12.061

[20] Kaniowski, R., & Pastuszko, R. (2021). Pool boiling of water on surfaces with open microchannels. *Energies*, 14, 3062. doi: 10.3390/en14113062

[21] Misale, M., & Bocanegra, J.A. (2023). Experiments and qualitative analysis by artificial neural network approach on pool boiling of FC-72 on finned surfaces confined by an unheated horizontal wall. *International Journal of Thermal Sciences*, 187, 108105. doi: 10.1016/j.ijthermalsci.2022.108105

[22] Rainey, K.N., & You, S.M. (2000). Pool boiling heat transfer from plain and microporous, square pin-finned surfaces in saturated FC-72. *Journal of Heat Transfer*, 122(3), 509–516. doi: 10.1115/1.1288708

[23] Kumar, U., Suresh, S., Thansekhar, M.R., & Babu, D. (2017). Effect of diameter of metal nanowires on pool boiling heat

transfer with FC-72. *Applied Surface Science*, 423, 509–520. doi: 10.1016/j.apsusc.2017.06.135

[24] Yu, C.K., & Lu, D.C. (2007). Pool boiling heat transfer on horizontal rectangular fin array in saturated FC-72. *International Journal of Heat and Mass Transfer*, 50, 3624–3637. doi: 10.1016/j.ijheatmasstransfer.2007.02. 003

[25] Cooke, D., & Kandlikar, S.G. (2012). Effect of open microchannel geometry on pool boiling enhancement. *International Journal of Heat and Mass Transfer*, 55, 1004–1013. doi: 10.1016/j.ijheatmasstransfer.2011.10. 010

[26] Gouda, R.K., Pathak, M., Khan, & Mohd., K. (2018). Pool boiling heat transfer enhancement with segmented finned microchannels structured surface. *International Journal of Heat and Mass Transfer*, 127, 39–50. doi: 10.1016/j.ijheatmasstransfer.2018.06.115

[27] Walunj, A., & Sathyabhama, A. (2018). Comparative study of pool boiling heat transfer from various microchannel geometries. *Applied Thermal Engineering*, 128, 672–683. doi: 10.1016/j.applthermaleng.2017.08.157